ELSEVIER

Journal of Molecular Structure 595 (2001) 209–224

Journal of
MOLECULAR
STRUCTURE

www.elsevier.nl/locate/molstruc

Conformational analysis of octa- and tetrahalogenated tetraphenylporphyrins and their metal derivatives

M. Gruden[a], S. Grubišić[a], A.G. Coutsolelos[b], S.R. Niketić[a,*]

[a]*Department of Chemistry, Faculty of Science, University of Belgrade, P.O. Box 158, Studentski trg 16, YU-11001 Belgrade, Yugoslavia*
[b]*Department of Chemistry, University of Crete, GR-71409 Heraklion, Crete, Greece*

Received 2 January 2001; revised 14 February 2001; accepted 14 February 2001

Abstract

A new maximally diagonal force field for molecular modelling of metalloporphyrins is developed and optimized on the crystal structures of nickel(II) porphine, nickel(II) mono-*tert*-butylporphyrin and nickel(II) di-*tert*-butylporphyrin. It is then used to investigate non-planar distortions of octa- and tetrachloro tetraphenylporphyrins (TPP) and their Ni(II) and Tb(III) complexes. Molecular mechanics (MM) calculations reproduced very well the structure of Tb(III) octachloro-TPP (so far the only example of a crystallographically characterized chloro TPP metal derivative). Normal-coordinate structural decomposition (NSD) analysis was performed on the equilibrium structures obtained by MM calculations. As expected, *sad* distortion dominates in octachloro structures irrespective of the presence or the size of the central metal atom; *dom* distortion dominates in tetrachloro structures with large Tb(III) central atom, while *sad*, *ruf*, *wav* and *pro* distortions are present in various amounts in other tetrachloro structures (TPP free base and Ni(II) complex) depending on the pattern of peripheral chloro substitution on the pyrrole rings. Other observed regularities are: reduction of the conformational flexibility of the porphyrin core upon metallation, and increase of the dihedral angle between the phenyl groups and the mean LSQ plane of the porphyrin core, as well as the overall increase in structural regularity upon the increase of the size of the central metal atom.

Keywords: Molecular mechanics; Porphyrins; Porphyrin conformations; Normal-coordinate structural decomposition; Ni(II) porphyrin complexes; Tb(III) porphyrin complexes

1. Introduction

Significant nonplanar distortions of the porphyrin macrocycle, observed in X-ray crystal structures of most hemoproteins, are believed to have important biological relevance [1].

The porphyrin macrocycle displays a range of distorted nonplanar shapes [2–5], which are presumably caused by different protein environments surrounding the porphyrin. This is based on evidence showing that the isolated heme group is nearly planar in solution environments, and that external forces must be applied to cause significant nonplanar distortion [6].

The nonplanar distortions of metalloporphyrins can be classified (Fig. 1) according to the irreducible representations of the nominal D_{4h} point group of a planar porphyrin [7,8]. The commonly observed *ruf* and *sad* distortions resemble the lowest-frequency normal coordinates of B_{1u} and B_{2u} symmetry, respectively, whereas *dom* and *wav* distortions are similar to

* Corresponding author. Fax: +381-11635-425.
E-mail address: nik@chem.bg.ac.yu (S.R. Niketić).

0022-2860/01/$ - see front matter
PII: S0022-2860(01)00550-6

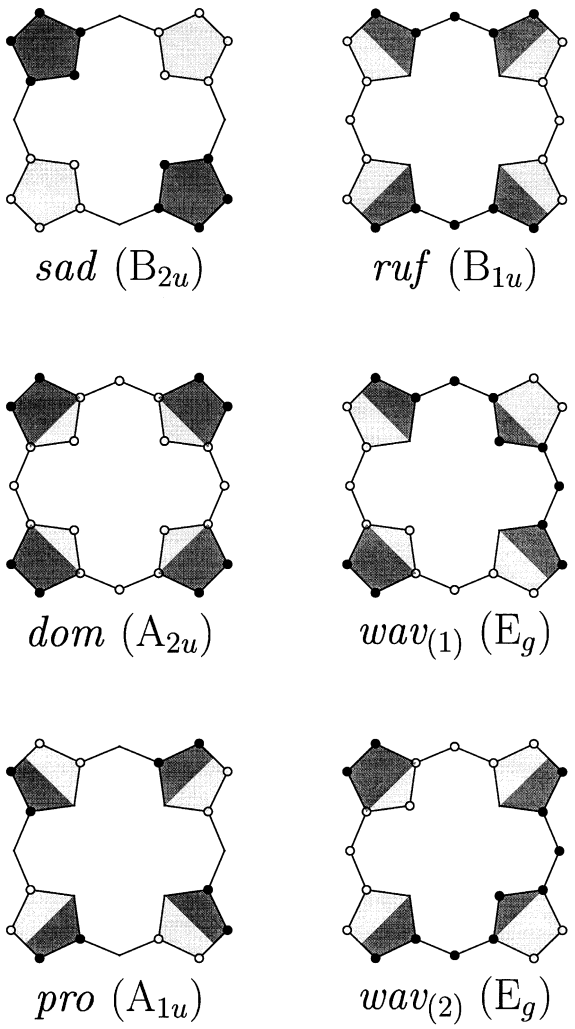

Fig. 1. Non-planar porphyrin-core conformations with standard labels (*sad* = saddle, *ruf* = ruffle, *wav* = wave, and *dom* = dome) and the respective symmetries. Open and closed circles represent core atoms lying below and above the mean plane. Light and dark segments represent parts of the pyrrole rings lying below and above the mean plane, respectively.

the lowest-frequency normal coordinates of A_{2u} and E_g symmetries. This suggests that a convenient way to describe these structures is in terms of the displacement along the lowest-frequency normal coordinates. For symmetrically substituted porphyrins, a nonplanar distortion usually occurs along one of the lowest-frequency normal coordinates given a particular configuration of the substituents. For an asymmetrically substituted porphyrin a more complicated nonplanar distortion may occur, which can be represented in terms of a linear combination of displacements along the lowest-frequency normal deformations [9].

Theoretically, the complete set of normal coordinates for a macrocycle forms a basis for describing any distortion of a porphyrin core. For a macrocycle of D_{4h} symmetry the distortions can be divided into in-plane and out-of-plane deformations. Only a few of the lowest-frequency modes are required to describe the out-of-plane distortions adequately [10], since these are the softest modes of deformation of the porphyrin. That is, the restoring forces for displacements along these coordinates require least energy. Since the lowest-frequency B_{2u} and B_{1u} modes usually appear at a lower frequency than the lowest-frequency A_{2u} mode, *sad* and *ruf* distortions are observed more frequently than *dom* distortion. The lowest-frequency mode of A_{1u} symmetry, *pro* (propellering of the pyrroles), is so high in frequency that *pro* deformation is rarely observed.

In order to investigate the roles of these different types of nonplanar porphyrin distortions in biological systems, it is useful to design and study models of porphyrins that have conformations similar to those found in the proteins.

The factors that influence the structure of a macrocycle can be classified into one of four basic categories [11]: peripheral substitution, the central metal, axial ligation, and the environment of the porphyrin. Peripheral substitution includes the substitution pattern (the number and sites of substituents), the substituent orientations, and other substituent properties (steric shape and size, electronic properties). The central metal may vary in electronic nature and in size.

We have been studying the effects of the peripheral substitution and the nature of the central metal atom on nonplanar distortions of porphyrins. The steric effects of substituents have been explored by studying three series of octa- and tetrachloro tetraphenyl substituted porphyrins. The metal dependence of nonplanar distortions was studied by examining the series of substituted porphyrins without metal, and with Ni(II) and Tb(III) as representative small and large transition metal ions, respectively.

2. Halogeno substituted tetraphenylporphyrins and related systems

Halogeno substituted porphyrins have been studied by various experimental techniques. Crystal structures have been reported for octabromo tetrachloro tetraphenylporphyrins (TPP) derivatives with Zn(II) [12] and Fe(II) [13], and for octafluoro TPP structure with Zn(II) [14]. Other reports dealing with octahalogenated porphyrins comprise the crystal structures of tetrakis(pentafluorophenyl) or tetramesityl octabromo derivatives with Zn(II) [15], Cu(II) [16], Ni(II) [17,16], Fe(III) [18,19], Fe(II) [19], as well as octachloro derivatives with Cu(II) [20], Fe(III) [18], Ru(II) [21], and Zn(II) [22]. The only example of a crystallographically characterized octachloro TPP derivative seems to be a Tb(III) structure reported recently by one of us [23].

For tetrahalogenated derivatives there are only a few structural results, all pertaining to tetrabromo TPP derivatives of: Zn(II) [24], Fe(III) [25], and Ni(II) [26]. It is noteworthy that all these structures represent 2,3,12,13-tetrabromo isomer, which is denoted as *ct* in this paper (see Fig. 2) in distinction from the *tt* isomer substituted in the positions 2,8,12,18.

Molecular mechanics (MM) calculations have previously been used by several other groups [11,27,28] to predict the conformations of metalloporphyrins. We used MM calculations to predict the stable conformations for the series of halogenated porphyrins mentioned above. The conformers obtained by MM calculations are stereochemically characterized, compared with available X-ray crystal structures, and analyzed by the normal-coordinate structural decomposition (NSD) method.

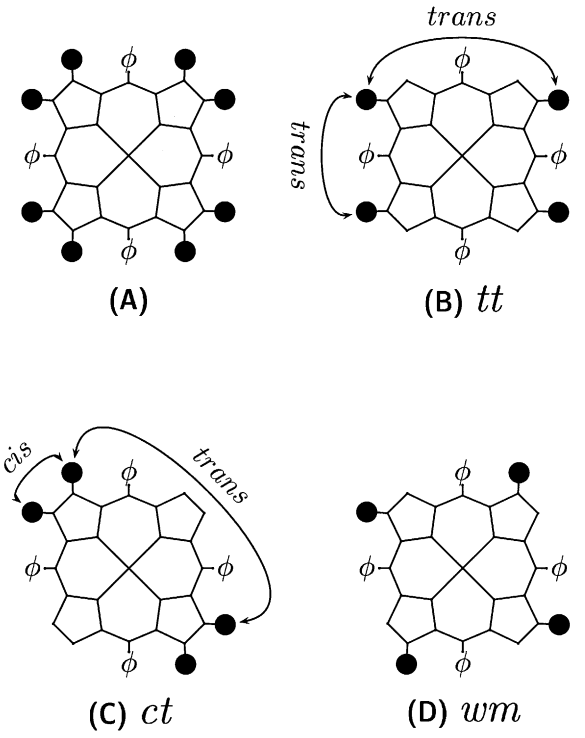

Fig. 2. Halogeno-substituted TPP investigated in this work. Large black circles represent the halogen substituents: (A) 2,3,7,8,12,13,17,18-octahalogeno-TPP; (B) 2,8,12,18-tetrahalogeno-TPP, *trans–trans* or *tt* isomer (symmetry D_2); (C) 2,3,12,13-tetrahalogeno-TPP, *cis–trans* or *ct* isomer (symmetry D_2); (D) 2,7,12,17-tetrahalogeno-TPP, *windmill* or *wm* isomer (symmetry C_{4h}).

3. Molecular mechanics calculations

Molecular energy optimization calculations were carried out using the consistent force field (CFF) conformation program [29]. The force field is of a maximally diagonal type. The energy is calculated from the equation presented in Scheme 1 (force field energy expression).

3.1. Force field parametrization

The force field is parametrized on the basis of the four different types of carbon atom (α and β pyrrole carbons, *meso* carbon of the porphyrin ring, and aromatic carbon of the phenyl substituents), one type of hydrogen and of nitrogen, the central metal atom (where applicable), and the halogen substituents treated as chlorine atoms.

The force field was developed on the chosen reference structures (see the next section) by adjusting appropriate parameters on a trial-and-error basis until the rmsd's between calculated and crystallographically observed bond lengths and valence angles were $\leq$0.01 Å and $\leq$2°, respectively. Torsional angles were reproduced to $\ll$ 4° in most cases.

Currently there are two approaches to representing metal–ligand (M–L) bonds in MM calculations [30].

In the 'bonded' approach the M–L bond is treated as a covalent bond defined by the force field parameters corresponding to the ideal bond lengths or angles and the appropriate force constants. In the 'nonbonded' approach the M–L bond is treated using electrostatic and van der Waals terms. The choice of the model depends on the nature of the problem to be investigated, with each approach having distinct advantages in different situations [31].

Bond-stretching and angle-bending contributions were treated with simple harmonic functions (that is, retaining quadratic terms only) and this approach proved to be quite adequate for the present study.

We have chosen the 'bonded model' for the treatment of metal–ligand interactions. In this way we were able to model the changes in the size of the central metal atom in a straightforward way and without loosing the capability to compare the stretching parameters with the corresponding vibrational force-constants in a simple manner. Furthermore, both our previous experience [32] on octahedral chelated transition metal structures and our ongoing other studies of multidentate and macrocyclic structures corroborate the advantages of the bonded model in cases where only the small changes in the coordination sphere are anticipated.

This model requires also the angle-bending functions for L–M–L deformations. For the treatment of the square-planar geometry of the coordination sphere it was necessary to include angle-bending functions both for *cis* and for *trans* L–M–L angles around the metal. Our program assigns θ_0 at π or $\pi/2$ for *trans* or *cis* L–M–L angles, respectively. Furthermore, k_θ (*cis*) is different from k_θ (*trans*) (see Table 2). In this way, we were able to control the stereochemistry of the coordination sphere without the need for out-of-plane bending functions or similar constructs.

Torsional contributions were taken for all possible combinations of the terminal atoms for a given bond (that is, a sum of four torsions involving a double bond, or nine torsions involving a single bond between two tetrahedrally coordinated atoms was considered). The heights of individual torsional barriers for a given bond were the same and were chosen so that their sum corresponded to the effective overall barrier. In this way, the apparent redundancy of the torsional parameters was minimized, and the need for out-of-plane bending functions was again eliminated.

$$E_{total} = \sum_r \tfrac{1}{2}k_r(r-r_0)^2 + \sum_\theta \tfrac{1}{2}k_\theta(\theta-\theta_0)^2 + \sum_\phi \tfrac{1}{2}k_\phi(1+\cos n\phi) + \sum_{ij}\left[\tfrac{2}{3}\epsilon\left(\frac{r^*}{r}\right)^9 - \epsilon\left(\frac{r^*}{r}\right)^6\right] + \sum_{ij}\frac{e_i \cdot e_j}{D \cdot r_{ij}}$$

Scheme 1.

Non-bonded contributions were computed with the Lennard–Jones '9-6' type function. Initial values for nonbonded parameters were adjusted to fit the functions taken over from our earlier work on ammine [33] and aminocarboxylato [34] transition metal complexes, where applicable. Other parameters for porphyrin-specific nonbonded interactions were then chosen by extrapolation on the basis of several widely available parameter sets imposing their consistency with our original force-field [33,34]. 1,3 nonbonded interaction were excluded from the calculations.

Point charges were obtained from simple semiempirical MO calculations [35]. PC adaptation and extension [36,37] of the Hoffmann's SIMCON program was employed for these calculations. In the evaluation of the electrostatic contributions to the E_{total} the distance dependent dielectric constant (D) was used.

3.2. Preliminary refinement of the force field

The force field parameters corresponding to the strain-free bond length and valence angle values were systematically varied to obtain the closest possible match of the calculated structures of nickel(II) porphine (NiP), nickel(II) mono-*tert*-butylporphyrin (NiMtBuP), and nickel(II) di-*tert*-butylporphyrin (NiDtBuP) with the crystal structures [9,11,38]. At the same time our results were compared to those of Song et al. [11]. The torsional and nonbonded parameters were likewise refined during this stage, mainly in order to obtain the porphyrin core puckering of the same magnitude as in the representative crystal structures, but also to improve the consistency of the entire force field.

Structural parameters for the resulting energy-minimized conformers are listed in Table 1. Our

Table 1
Selected average bond lengths (Å) valence angles (°) and torsional angles (°) for Nickel(II) porphine, Nickel(II) mono-*tert*-butylporphyrin, and Nickel(II) 5,15-di-*tert*-butylporphyrin

	Ni–N	C_β–C_β	C_α–C_m	C_α–N	N–Ni–N	C_α–N–C_α	N–C_α–C_β–C_β	N–C_α–C_m–Cα
NiP								
Calculated[a]	1.930	1.337	1.369	1.376	180.0	104.8	0.0	0.0
X-ray[b]	1.951	1.347	1.371	1.379	179.3	104.3	0.3	0.8
Song X. et al.[c]	1.944	1.330	1.372	1.379	180.0	104.2	0.0	0.0
NiMtBuP								
Calculated[a]	1.917	1.338	1.372	1.377	177.3	105.2	4.5	14.3
X-ray[b]	1.901	1.342	1.380	1.380	178.9	106.3	3.0	11.1
Song X. et al.[c]	1.914	1.333	1.380	1.377	178.0	105.2	2.3	13.8
NiDtBuP								
Calculated $\alpha\alpha$[a]	1.900	1.341	1.379	1.373	177.6	106.0	5.4	25.1
Song X. et al. $\alpha\alpha$[c]	1.892	1.334	1.387	1.376	175.9	106.0	2.0	20.5
X-ray[b]	1.900	1.353	1.394	1.383	177.0	106.2	2.9	14.8
Calculated $\alpha\beta$[a]	1.910	1.337	1.378	1.377	179.9	103.9	6.1	19.1
Song X. et al. $\alpha\beta$[c]	1.928	1.329	1.383	1.380	180.0	104.8	5.5	21.2

[a] Our energy minimized structures.
[b] X-ray crystal structures.
[c] Energy minimized structures from Ref. [11].

calculate energy distribution is in good agreement with the results of Song et al. [11]. As expected, the $\alpha\alpha$ conformer of NiDtBuP proved to be more stable than the $\alpha\beta$ conformer. Fig. 3 shows the atom types that were used for parametrization, whereas Table 2 lists all the force field parameters.

3.3. Computational procedure

All the stable conformers for the series of porphyrins were obtained by energy minimization of the four initial structures (*dom*, *sad*, *wav*, and *ruf*) representing the idealized normal deformations of the porphyrins core. They were generated from standard bond lengths, valence angles, and the corresponding *z*-coordinate displacements (as shown in Fig. 1). In addition, all meaningful combinations of phenyl group orientations were investigated. The phenyl substituents were not treated as part of the same delocalized system as the core. If they were, the C_m–C_p torsional constants between the porphyrin core and phenyl substituents would have been too large. It was therefore necessary to redefine the carbon atoms of the phenyl ring (atom C_p in Table 2) and to use different parameters to describe the phenyl rings, and also to treat C_m–C_p bonds as essentially single. In this way, it was possible to model the partially hindered rotations of the phenyl rings with respect to the porphyrin core.

Geometry optimizations were carried out using the combination of steepest-descent, Fletcher–Powell and Newton–Raphson methods. Steepest-descent and Fletcher–Powell methods were mostly used in that order for initial exploratory searches and minimizations of conformations far from equilibrium. The number of iterations varied widely in optimization experiments. In particularly difficult cases it was necessary to alternate between these two procedures more than once. To approach true minima Newton–Raphson iterations were always employed. Geometry optimizations were carried down to the rms gradient of $<10^{-6}$ kJ/mol Å.

By judicious combination of the three minimization algorithms it was possible to optimize the geometry of every structure studied in this work. It is noteworthy that in all cases a unique equilibrium conformation was impeccably reached regardless of the initial conformation (*dom*, *sad*, *wav*, or *ruf*) which process sometimes required rather lengthy (in terms of the number of iterations) transitions in the conformational space from one of the normal-mode conformations into another. However, this fact substantiated the

Table 2
CFF parameters for porphyrins

Bond stretching parameters

	k_r (kcal/mol Å^2)	r_0 (Å)
M–N	359.50	1.910 (2.360)[a]
N–C_α	1594.74	1.375
C_α–C_β	1380.48	1.337
C_α–C_α	1380.48	1.337
C_β–H	661.00	1.101
N–H	805.28	1.011
C_β–Cl	487.48	1.720
C_p–C_p	138.48	1.394
C_p–H	661.80	1.084
C_p–C_m	632.72	1.497
C_m–C_α	1409.24	1.370

Angle bending parameters

	k_θ (kcal/mol rad^2)	θ_0 (rad)
N–M–N (*cis*)	5.00	1.571
M–N–C_α	129.60	2.182
C_α–C_β–H	51.84	2.094
C_β–C_β–H	51.84	2.094
N–C_α–C_β	61.92	1.900
C_α–C_β–C_β	61.92	1.872
C_m–C_α–C_β	61.92	2.094
C_β–C_β–Cl	134.00	2.094
C_α–C_m–C_p	61.92	2.094
C_α–C_β–H	51.84	2.094
N–M–N (*trans*)	30.32	3.146
C_α–N–C_α	61.92	1.832
C_p–C_p–H	51.84	2.094
C_p–C_p–C_m	61.92	2.094
C_α–C_m–C_α	61.92	2.120
N–C_α–C_m	61.92	2.175
C_α–C_β–Cl	134.00	2.094
C_p–C_p–C_p	61.92	2.094
C_α–N–H	51.84	2.094
C_β–C_β–H	51.84	2.094

Electrostatic parameters

	esu
M	0.543
Cl	−0.315
C_α	0.285
C_p	−0.080
N	−0.665
C_m	0.334
C_β	0.285
H	0.285

Torsional parameters

	k_ϕ (kcal/mol)	n
C_m–C_α–N–M	1.57	−2.0
C_α–C_β–C_β–C_α	3.00	−2.0
H−C_β–C_β–C_α	3.00	−2.0
C_p–C_p–C_m–C_α	0.50	−2.0
C_m–C_p–C_p–H	7.50	−2.0
Cl–C_β–C_β–Cl	3.00	−2.0
Cl–C_β–C_β–H	3.00	−2.0
C_α–N–C_α–C_m	3.00	−2.0
C_β–C_α–N–H	3.00	−2.0
C_β–C_β–C_α–C_m	10.00	−2.0
H–C_β–C_β–H	3.00	−2.0
C_p–C_m–C_α–C_β	10.00	−2.0
C_p–C_p–C_p–C_p	7.50	−2.0
H–C_p–C_p–H	7.50	−2.0
Cl–C_β–C_β–C_α	3.00	−2.0
H–C_β–C_β–C_α	3.00	−2.0
C_m–C_α–N–H	3.00	−2.0

van de Waals parameters

	ϵ (kcal/mol)	r^* (Å)
M–C_β	0.130	3.24
M–C_m	0.130	3.24
M–C_p	0.130	3.24
N–C_β	0.049	3.76
N–C_m	0.049	3.76
C_α–C_β	0.044	3.88
C_β–C_β	0.044	3.88
C_m–C_α	0.046	3.88
C_p–C_p	0.044	3.88
H–C_β	0.046	3.34
Cl–C_β	0.103	3.97
Cl–Cl	0.240	4.00
Cl–C_m	0.103	3.97
H–C_p	0.046	3.34
C_p–C_m	0.044	3.88
C_p–C_β	0.044	3.88
C_p–Cl	0.103	3.97
M–H	0.134	2.70
M–Cl	0.115	3.28
N–H	0.051	3.32
N–C_α	0.049	3.76
H–H	0.047	3.00
C_α–C_α	0.044	3.88
C_m–H	0.046	3.34
C_m–C_β	0.046	3.88
N–Cl	0.115	3.85
H–C_α	0.046	3.34
Cl–C_α	0.103	3.97
H–Cl	0.106	3.53
N–N	0.055	3.64
C_p–C_p	0.044	3.88
C_p–C_α	0.044	3.88
C_p–N	0.049	3.74

[a] Unconstrained bond distances for Ni(II), and for Tb(III) (in parantheses).

geometry optimization results and practically eliminated any possibility that we reached a weak or a local minimum.

Ortep III [39] (Windows version [40]) was used to

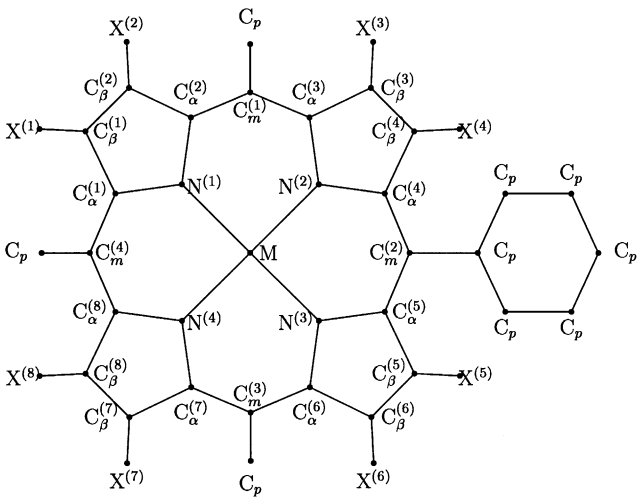

Fig. 3. Atom types used in defining the force field parameters for molecular mechanics calculation. For clarity, only one phenyl ring is shown. Positions denoted by X are either hydrogens or halogens.

draw energy-minimized structures. Van Zandt's package [41] coupled with locally written FORTRAN programs was used to produce cylindrical plots of porphyrin core conformations, and other drawings.

3.4. Normal-coordinate structural decomposition

For each of the equilibrium structures obtained by the energy minimization procedure we have carried the normal-coordinate structural decomposition of the out-of-plane deformation into the six basic symmetry types (*dom*, *sad*, $wav_{(x)}$, $wav_{(y)}$, *ruf*, and *pro*) [10]. For the purpose of this work, we have followed a simplified procedure based on the projection-operator approach. The projection-operator (24×24) matrices were constructed from the normalized non-mass-weighted eigenvectors, $|z\rangle$, describing the z-coordinate displacements of each of the six basic symmetry types ($wav_{(x)}$ and $wav_{(y)}$ were the two components of the doubly-degenerate E_g normal coordinate), as $|z\rangle\langle z|$.

The energy minimized structures were transformed into a standard form by translating the cartesian coordinates into the centre of mass space, calculating the weighted least-squares plane through the core atoms of the macrocycle (excluding the central metal atom, where applicable) [42,43], and by rotating the structure so that the vector normal to the least-squares plane coincides with the z-axis of the coordinate system. Then the projection operators were applied, in turn, on the z coordinate displacement vector, $|\xi\rangle$, yielding the corresponding coefficients, C_ξ, in the linear combination of the normal coordinates comprising the basis set:

$$|z\rangle\langle z|\xi\rangle = C_\xi|\xi\rangle$$

under the assumption that the basis set $\{|z\rangle\}$ is orthogonal (which it is, since each $|z\rangle$ transforms as an irreducible representation of D_{4h} point group), and that it fairly completely spans the space of normal-mode deformations.

The validity of this approach was checked using the X-ray structure of Ni(II) 5,15-di-*tert*-butylporphyrin [9] for which the normal-coordinate structural decomposition was done by Shelnutt et al. [9], as well as on a series of porphyrin structures of cytochromes [44] using the coordinates deposited in PDB [45]. In all cases our calculated contributions of the six basic out-of-plane normal coordinates were in remarkable agreement with the values reported in Shelnutt et al. [46] or in the Shelnutt's NSD Database Search Engine [47].

4. Results

Results are presented for the twelve structures

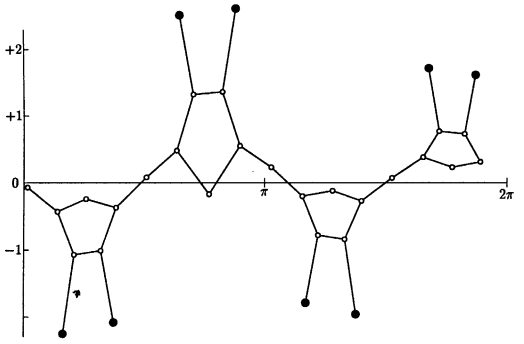

H_2-TPP-Cl_8.

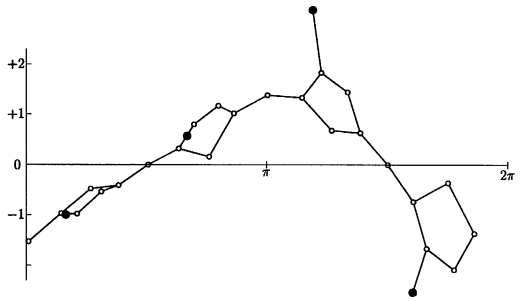

H_2-TPP-*wm*-Cl_4.

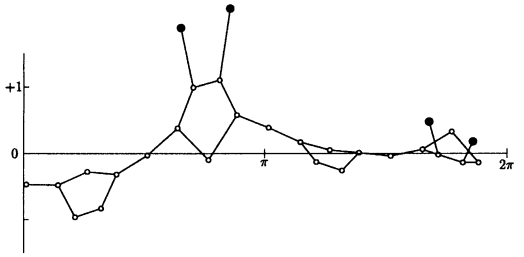

H_2-TPP-*ct*-Cl_4.

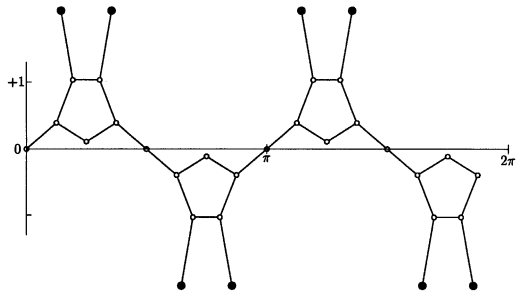

Ni(II)-TPP-Cl_8.

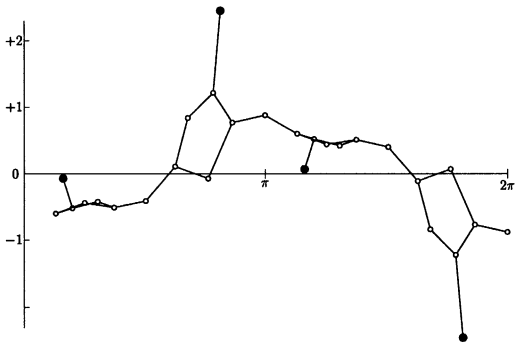

H_2-TPP-*tt*-Cl_4.

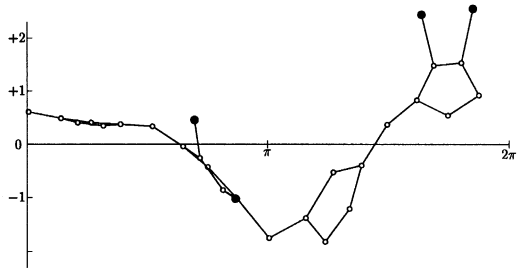

Ni(II)-TPP-*ct*-Cl_4.

Fig. 4. Cylindrical projections of octa- and tetra-chloro free-bases Ni(II) and Tb(III) complexes. The horisontal axis shows azimuthal angle, and the vertical axis shows *z*-coordinate displacement (in Å) relative to the *xy*-plane containing the central metal atom.

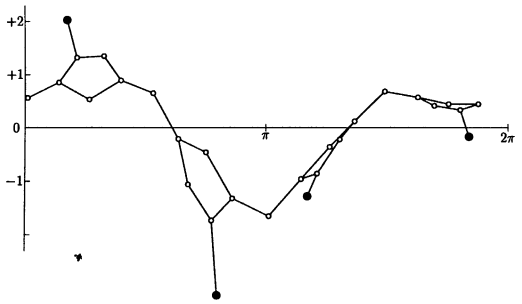

Ni(II)-TPP-*tt*-Cl_4.

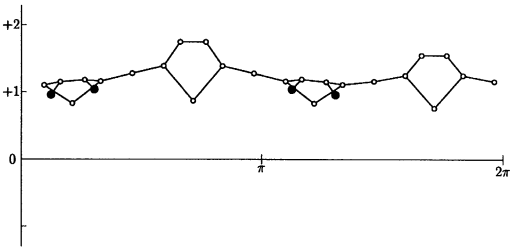

Tb(III)-TPP-*ct*-Cl_4.$^+$

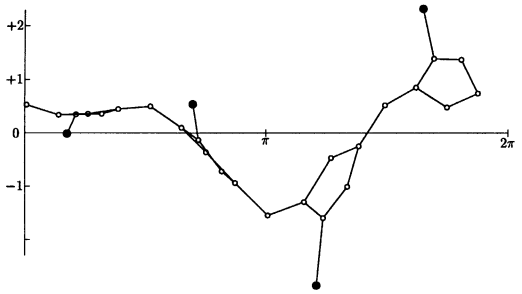

Ni(II)-TPP-*wm*-Cl_4.

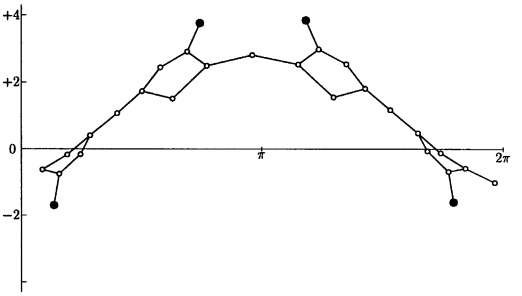

Tb(III)-TPP-*tt*-Cl_4.$^+$

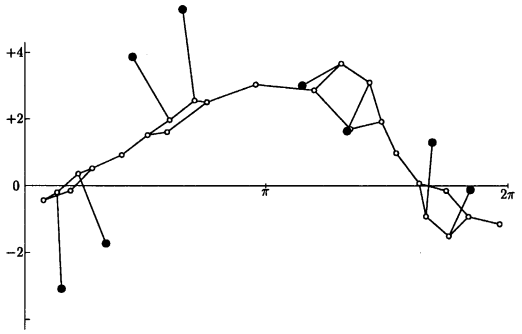

Tb(III)-TPP-Cl_8.$^+$

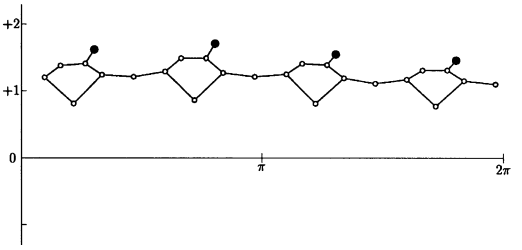

Tb(III)-TPP-*wm*-Cl_4.$^+$

Fig. 4. (*continued*)

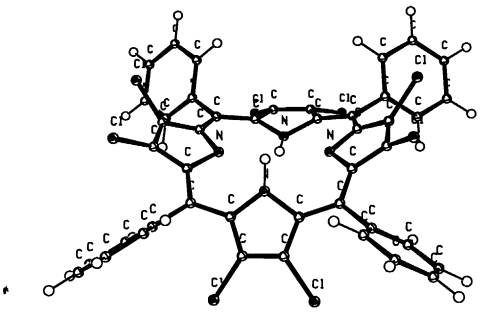

H_2-TPP-Cl_8.

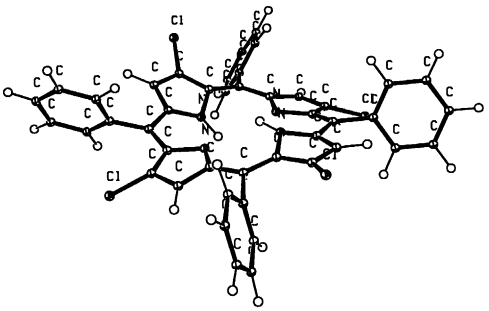

H_2-TPP-*wm*-Cl_4.

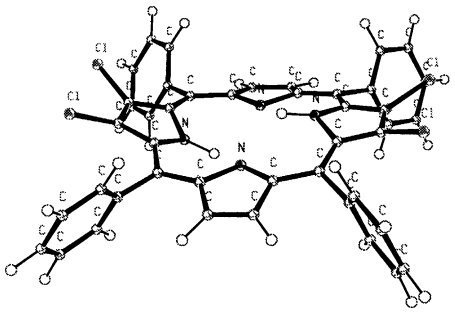

H_2-TPP-*ct*-Cl_4.

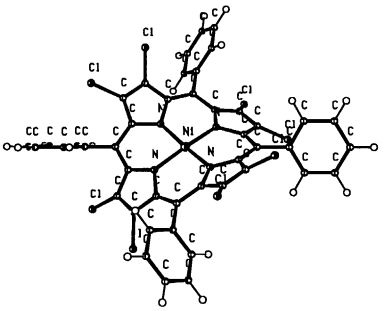

Ni(II)-TPP-Cl_8.

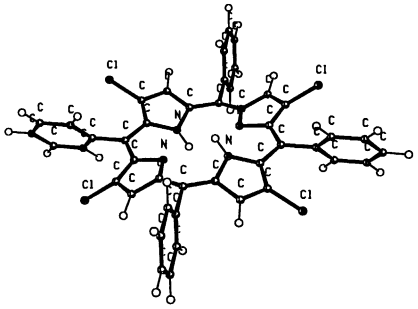

H_2-TPP-*tt*-Cl_4.

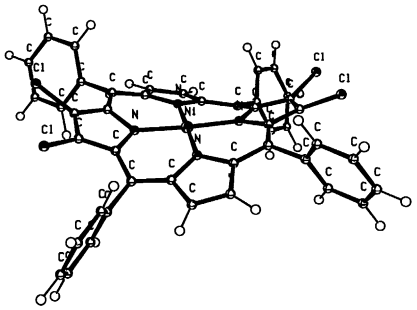

Ni(II)-TPP-*ct*-Cl_4.

Fig. 5. ORTEP Illustrations of the equilibrium conformations of X_8 and X_4-TPP free-base, Ni(II) and Tb(III) complex.

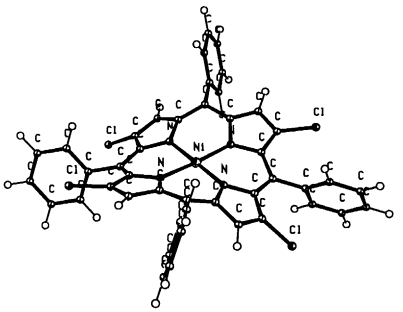

Ni(II)-TPP-*tt*-Cl_4.

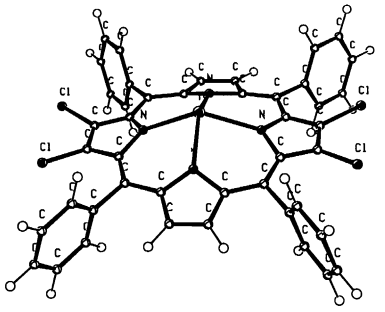

Tb(III)-TPP-*ct*-Cl_4^+.

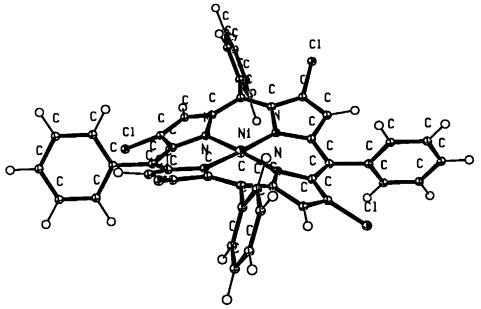

Ni(II)-TPP-*wm*-Cl_4.

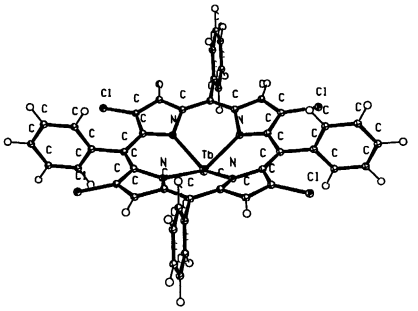

Tb(III)-TPP-*tt*-Cl_4^+.

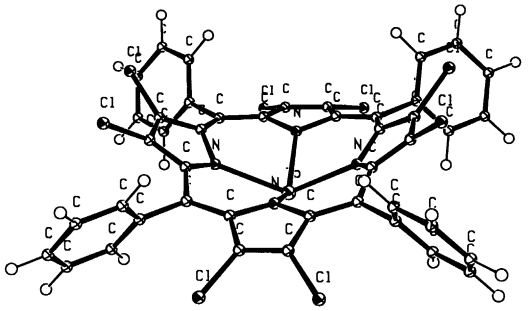

Tb(III)-TPP-Cl_8^+.

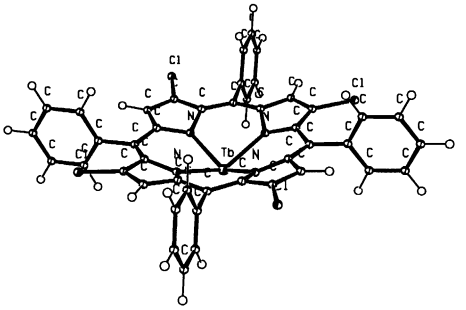

Tb(III)-TPP-*wm*-Cl_4^+.

Fig. 5. (*continued*)

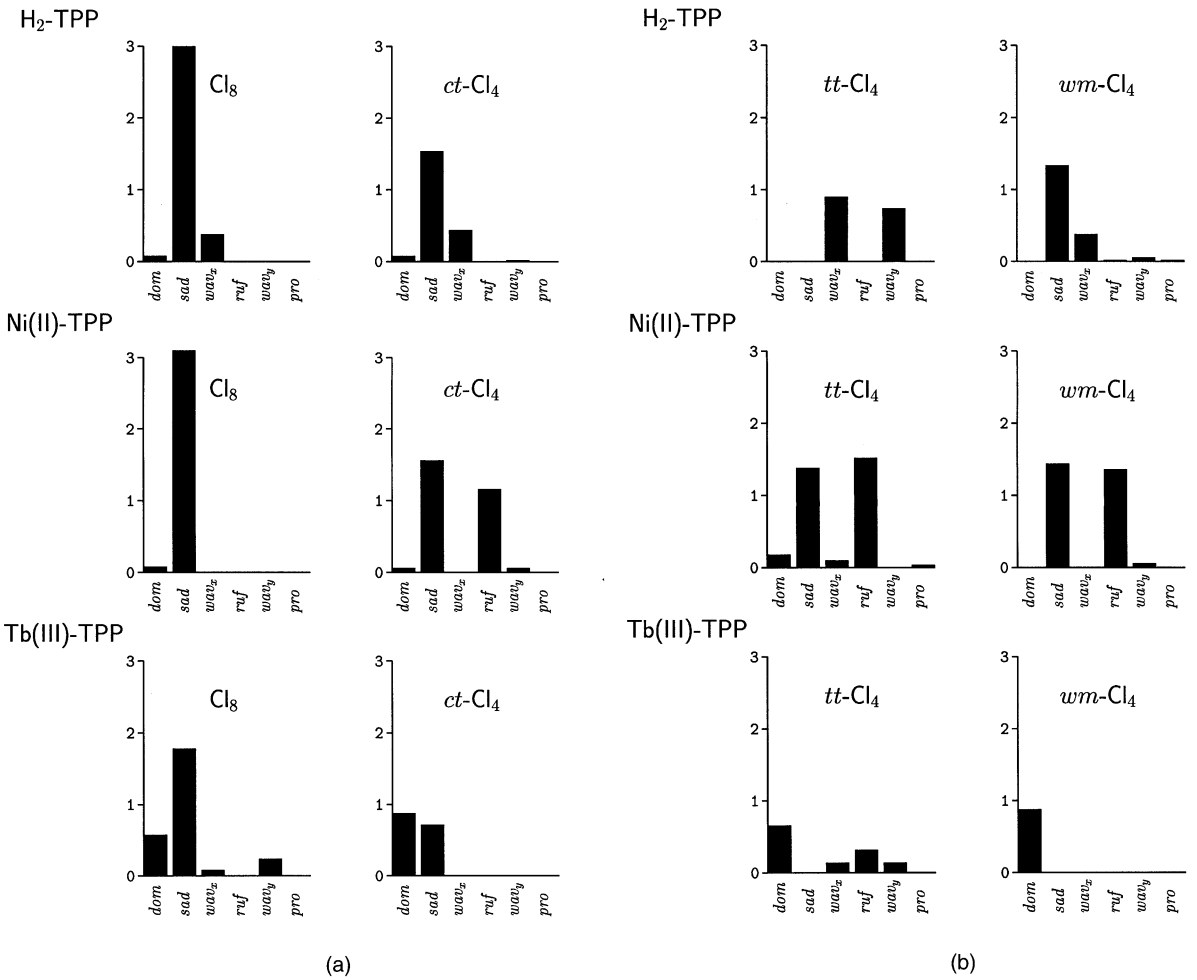

Fig. 6. Results of the normal-coordinate structural decomposition (NSD Analysis) for the equilibrium conformations of octa- and tetra-chloro derivatives of TPP free-base, Ni(II) complex, and Tb(III) complex.

studied in this work, i.e. one octachloro and three tetrachloro isomers for the free-base H_2TPP, TPP-Ni(II), and TPP-Tb(III)$^+$ complexes, as follows. Fig. 4 shows the cylindrical projections perpendicular to the *z*-axis of a coordinate system in which the weighted least-squares plane through all core atoms coincides with the *xy*-plane. Fig. 5 then shows ORTEP illustrations of all equilibrium structures. Finally, the results of normal-coordinate structural decomposition (NSD) for all equilibrium structures is summarized in Fig. 6.

4.1. Octachloro derivatives

It was found that in the case of Cl_8TPP free-base, Cl_8TPP-Ni(II) and Cl_8TPP-Tb(III) the energy minimization and geometry optimization procedure resulted in one single stable conformation for each porphyrin structure, regardless of the initial conformation we started with. The structural parameters for the energy-minimized conformers are presented in Table 3 and the calculated energy distributions for all conformers are listed in Table 4.

Table 3
Selected average values for bond lengths (Å) and valence angles (°) of the equilibrium TPP structures

	Ni–N	C_β–C_β	C_α–C_m	C_α–N	N–Ni–N	C_α-N-C_α
Free base TPPH$_2$						
Cl_8		1.344	1.378	1.382		105.8
wm-Cl_4		1.339	1.377	1.382		104.5
tt-Cl_4		1.340	1.378	1.382		105.5
ct-Cl_4		1.340	1.377	1.380		103.9
TPP–Ni(II)						
Cl_8	1.883	1.342	1.376	1.380	173.2	105.6
wm-Cl_4	1.887	1.343	1.375	1.378	176.7	106.3
tt-Cl_4	1.885	1.346	1.376	1.382	176.8	106.7
ct-Cl_4	1.892	1.342	1.375	1.381	176.5	105.7
TPP–Tb(III)$^+$						
Cl_8	2.300	1.344	1.384	1.383	131.2	108.8
wm-Cl_4	2.302	1.342	1.383	1.379	138.7	108.8
tt-Cl_4	2.303	1.342	1.383	1.379	138.1	108.8
ct-Cl_4	2.301	1.343	1.383	1.379	138.3	108.4

The skeletal deviations of the 24 core atoms from the average plane of the macrocycle are clearly discerned from the cylindrical projections (see Fig. 4).

The NSD analysis reveals that the structure of the Cl_8TPP free-base is a mixture of *sad*, $wav_{(x)}$, and *dom* deformations. The magnitude of saddle distortion is the largest. Structural data for the core conformation and the bond lengths and angles for Cl_8TPP–Ni(II) show that substituted porphyrins (Table 3) exhibit structural differences in comparison to the planar porphyrins (Table 1). This is evident in the shortening of Ni–N bond lengths and a decrease of the N–Ni–N angles. As can be seen from Fig. 4 the Cl_8TPP–Ni(II) shows large deviation from planarity, and NSD analysis points to an almost pure saddled macrocycle (Fig. 6). The porphyrin ring of Cl_8TPP–Tb(III) complex has a dominant saddle distortion with a small amount of *dom*, $wav_{(x)}$ and $wav_{(y)}$ distortions.

The geometry of the calculated structures is in good agreement with that of similar structures characterized by X-ray, which were available for comparison: octabromo derivatives of Ni(II) complexes (with mesityl instead of phenyl substituents on all C_m core carbons) [16,17,48] and the octachloro derivative of Tb(III) complex with TPP [23].

4.2. Tetrachloro derivatives

For Cl_4TPP free-base, Cl_4TPP–Ni(II) and Cl_4TPP–Tb(III), we obtained three stable conformations, one for each of the three symmetrically substituted geometrical isomers for each structure. The initial structures, chosen on the basis of the most symmetrical substitution pattern of the halogens, were: 2,8,12,18-tetrachloro-TPP, *trans–trans*, or *tt* isomer (Fig. 2(B)); 2,3,12,13-tetrachloro-TPP, *cis–trans*, or *ct* isomer (Fig. 2(C)), and 2,7,12,17-tetrachloro-TPP, *windmill*, or *wm* isomer (Fig. 2(D)), assuming that these isomers represent the most likely products in the partial halogenation reactions. Again, regardless of the initial conformation, only one stable conformer for each of the isomers is obtained. The structural parameters for the resulting energy-minimized conformers are presented in Table 3 and the calculated energy distributions for all conformers are listed in Table 4. The equilibrium structures are illustrated in Figs. 4 and 5.

The structures reported here for Cl_4TPP free base indicate that the porphyrins possess a high degree of conformational flexibility. Although the total energies of the three geometrical isomers are only slightly different, different amounts of normal distortion are observed. Isomer *ct* is a mixture of *sad*, $wav_{(x)}$, and *dom* deformations, whereas *wm* isomer is a mixture of *sad*, $wav_{(x)}$, *ruf*, $wav_{(y)}$ and *pro* deformations. In both of the structures *sad* deformation is dominant. In the

Table 4
Energy contributions (in kcal/mol) for the equilibrium TPP conformations

	E_{total}	E_{bond}	E_{angle}	$E_{torsion}$	E_{vdw}	E_c
Free base TPPH$_2$						
Cl_8	101.42	1.78	12.03	25.29	9.89	52.42
wm-Cl_4	44.65	1.28	12.56	13.35	10.05	7.41
tt-Cl_4	49.24	1.35	11.31	14.04	9.14	13.39
ct-Cl_4	55.75	1.43	11.74	14.42	12.12	14.04
TPP–Ni(II)						
Cl_8	36.74	1.38	12.21	23.70	2.13	−2.67
wm-Cl_4	−8.67	0.95	11.07	13.00	3.53	−37.23
tt-Cl_4	−4.58	1.16	12.36	12.19	3.26	−33.55
ct-Cl_4	2.34	0.89	11.05	13.64	3.99	−27.23
TPP–Tb(III)$^+$						
Cl_8	99.83	4.86	37.08	21.34	5.07	31.47
wm-Cl_4	51.02	3.94	32.75	8.47	3.76	2.10
tt-Cl_4	55.17	4.14	33.60	8.96	4.02	4.45
ct-Cl_4	62.18	4.03	31.91	9.84	4.81	11.60

Table 5
Dihedral angles (°) between the weighted least-square planes of the phenyl substituents (ϕ_i, $i = 1,4$) and the weighted least-squares plane of the core porphyrin macrocycle in the equilibrium TPP structures

TPP	*tt*-X_4	*ct*-X_4	*wm*-X_4	X_8
Free base TPPH$_2$				
ϕ_1	23.49	60.25	26.96	41.63
ϕ_2	75.89	60.25	47.05	41.61
ϕ_3	16.78	70.20	42.18	48.68
ϕ_4	77.08	70.44	23.81	48.79
TPP–Ni(II)				
ϕ_1	68.54	76.62	69.46	48.43
ϕ_2	74.47	76.62	69.46	48.43
ϕ_3	68.54	58.41	69.46	48.43
ϕ_4	74.47	58.41	69.46	48.43
TPP–Tb(III)$^+$				
ϕ_1	90.00	81.20	87.90	57.59
ϕ_2	90.00	81.20	87.90	57.59
ϕ_3	90.00	81.20	87.90	57.59
ϕ_4	90.00	81.20	87.90	57.59

case of *tt* isomer an almost equal ratio of $wav_{(x)}$ and $wav_{(y)}$ is observed (see Fig. 6).

However, for Cl_4TPP–Ni(II) the NSD analysis (Fig. 6) indicates that all three isomers are mixtures of the ruffle and saddle distortions with only the minor contributions from other distortion modes.

For the tetrachloro substituted structures with the very large Tb(III) ion a *dom* deformation is present in all of the three isomers, as expected. The *wm* isomer is generally dommed but for *tt* isomer the ruffle type of distortion (together with both $wav_{(x)}$ and $wav_{(y)}$) is also found, and for *ct* isomer the saddle distortion mode is found besides dome (Fig. 6).

5. Discussion and conclusions

The stability of tetrachloro substituted porphyrins depends upon the position of four Cl atoms. The highest energy is obtained for the isomer with two Cl atoms on the same pyrrole ring (that is, *ct* isomer) for Cl_4TPP–Ni(II) and Cl_4TPP–Tb(III). This result is in discord with the fact that only the *ct* isomer has been observed so far in crystal structure reports [24–26] pointing to the possibility that other than steric factors might predominately determine the course of partial halogenation of TPP structures, or that *ct* isomers crystallize more easily.

Since the porphyrins investigated in this work have sterically bulky groups at most or all of the peripheral positions of the macrocycle, the large distortions from planarity are expected. The free-base appears to be most flexible for all substitution patterns of halogens. This is reflected in the lack of symmetry of the equilibrium structures. In the substituted porphyrins, in which either the small Ni(II) ion or the very large Tb(III) ion are incorporated, additional effects on the distortion of the porphyrin core are expected. They are observed through different contributions of the normal-mode conformations obtained in the NSD analysis.

In conclusion, the series of structures studied in this work offered us a possibility to elucidate the concurrent effects of peripheral substitution and metallation on the non-planarity of porphyrins. Generally, metallation reduces the conformational flexibility. An increase of the radius of the central metal atom enhances the tetragonal symmetry of the porphyrin core. Furthermore, it renders the phenyl groups more perpendicular with respect to the mean porphyrin core plane (see Table 5). The substitution pattern in tetrachloro structures has an equally profound effect on the mode, extent, and symmetry of non-planar distortions, as discernible, for example,

Table 6
Dihedral angles (°) between the weighted least-square planes of pyrrole groups with the weighted least-square plane of the $C_{20}N_4$ core in the equilibrium TPP structures

TPP	*tt*-X_4	*ct*-X_4	*wm*-X_4	X_8
Free base TPPH$_2$				
$Pyrrol_1$	9.86	25.87	25.42	42.90
$Pyrrol_2$	22.21	13.44	6.45	22.89
$Pyrrol_3$	41.32	2.97	34.60	11.59
$Pyrrol_4$	22.81	13.46	29.68	22.87
TPP–Ni(III)				
$Pyrrol_1$	23.93	15.09	20.23	26.88
$Pyrrol_2$	17.93	27.34	20.23	26.88
$Pyrrol_3$	23.93	15.09	20.23	26.88
$Pyrrol_4$	17.93	27.34	20.23	26.88
TPP–Tb (III)$^+$				
$Pyrrol_1$	13.81	7.36	14.36	34.57
$Pyrrol_2$	13.81	21.54	14.36	9.47
$Pyrrol_3$	13.81	7.36	14.36	34.57
$Pyrrol_4$	13.81	21.54	14.36	9.47

Table 7
Displacement (in Å) of the chlorine atoms from the $C_{20}N_4$ weighted least-square plane in the equilibrium TPP structures

TPP	*tt*-X_4	*ct*-X_4	*wm*-X_4	X_8
Free base TPPH$_2$				
Cl_1	−1.872	1.528		2.370
Cl_2		1.531	1.474	2.368
Cl_3				−2.045
Cl_4	2.155		0.955	−2.099
Cl_5	−2.391	0.888		1.798
Cl_6		0.891	−1.686	1.796
Cl_7				−2.098
Cl_8	2.266		1.412	−2.042
TPP–Ni (II)				
Cl_1	−1.758	2.860		−2.057
Cl_2		2.860	1.506	−2.057
Cl_3				2.057
Cl_4	0.385		−1.506	2.057
Cl_5	−1.758	1.436		−2.057
Cl_6		1.436	1.506	−2.057
Cl_7				2.057
Cl_8	0.385		−1.506	2.057
TPP–Tb (III)$^+$				
Cl_1	0.080	0.217		2.004
Cl_2		0.217	−0.383	2.004
Cl_3				−1.305
Cl_4	0.080		−0.383	−1.305
Cl_5	0.080	0.217		2.004
Cl_6		0.217	−0.383	2.004
Cl_7				−1.305
Cl_8	0.080		−0.383	−1.305

from dihedral angles of pyrrole rings (Table 6), or axial displacements of the chlorine atoms (Table 7). The latter two tables show that both metallation and peripheral substitution (in terms of the number of substituents as well as the pattern of substitution) determine the non-planar conformation of a porphyrin in an intricate way as a resultant of several of mutually opposing strain relieving mechanisms.

6. Supplementary material available

Cartesian coordinates of all 12 equilibrium structures (octachloro, and *tt*, *ct*, and *wm* isomers of tetrachloro TPP as a free-base, Ni(II) and Tb(III) complex) in XYZ or PDB format can be downloaded from http://www.chem.bg.ac.yu/~nik.

Acknowledgements

This work has been financially supported by the Greek-Yugoslav Protocol for Scientific Cooperation through the respective Ministries of Science. MG and SRN were also partially supported by the Serbian Research Council through Grant No. 02E09. SG was supported by the State Labour Initiative project. We are grateful to the State Institute of Statistics, Belgrade, for the generous grant of computer time. To the fellow porphyrin chemists we owe our thanks for generously making their results available through www.

References

[1] M. Ravikanth, T.K. Chandrashekar, Struct. Bonding (Berlin) 82 (1995) 105.
[2] Y. Higuchi, M. Kusunoki, N. Yasuoka, M. Kakudo, J. Mol. Biol. 172 (1984) 109.
[3] G. Fermi, M.F. Perutz, B. Shaanan, R. Fourme, J. Mol. Biol. 175 (1984) 159.
[4] B.C. Finzel, T.L. Poulos, J. Kraut, J. Biol. Chem. 259 (1984) 13027.
[5] G.V. Louie, G.D. Brayer, J. Mol. Biol. 214 (1990) 527.
[6] K.K. Anderson, J.D. Hobbs, L. Luo, K.D. Stanley, J.M.E. Quirke, J.A. Shelnutt, J. Am. Chem. Soc. 115 (1993) 12346.
[7] X. Song, L. Jaquinod, W. Jentzen, D.J. Nurco, S.L. Jia, R.G. Khoury, J.G. Ma, C.J. Medforth, K.M. Smith, J.A. Shelnutt, Inorg. Chem. 37 (1998) 2009.
[8] W. Jentzen, M.C. Simpson, J.D. Hobbs, X. Song, T. Ema, N.Y. Nelson, C.J. Medforth, K.M. Smith, M. Veyrat, M. Mazzanti, R. Ramasseul, J.C. Marchon, T. Takencki, W.A. Goddard III, J.A. Shelnutt, J. Am. Chem. Soc. 117 (1995) 11085.
[9] X. Song, W. Jentzen, S.L. Jia, L. Jaquinod, D.J. Nurco, C.J. Medforth, K.M. Smith, J.A. Shelnutt, J. Am. Chem. Soc. 118 (1996) 12975.
[10] W. Jentzen, X. Song, J.A. Shelnutt, J. Am. Chem. Soc. 101 (1997) 1684.
[11] X. Song, W. Jentzen, L. Jaquinod, R.G. Khoury, C.J. Medforth, S.L. Jia, J.G. Ma, K.M. Smith, J.A. Shelnutt, Inorg. Chem. 37 (1998) 2117.
[12] P. Bhyrappa, V. Krishnan, M. Nethaji, J. Chem. Soc., Dalton Trans. (1993) 1901.
[13] D.S. Bohle, Chen-Hsiung Hung, J. Am. Chem. Soc. 117 (1995) 9584.
[14] J. LeRoy, A. Bondon, L. Toupet, C. Rolando, Chem.— A Eur. J. 3 (1997) 1890.
[15] R.E. Marsh, W.P. Schaefer, J.A. Hodge, M.E. Hughes, H.B. Gray, J.E. Lyons, P.E. Ellis Jr., Acta Crystallogr., Sect. C (Cr. Str. Comm.) C49 (1993) 1339.
[16] L.M. Henling, W.P. Shaefer, J.A. Hodge, M.E. Hughes, H.B.

Gray, J.E. Lyons, P.E. Ellis Jr., Acta Crystallogr., Sect. C (Cr. Str. Comm.) C49 (1993) 1743.
[17] D. Mandon, P. Ochsenbein, J. Fischer, R. Weiss, K. Jayaraj, R.N. Austin, A. Gold, P.S. White, O. Brigaud, P. Battioni, D. Mansuy, Inorg. Chem. 31 (1992) 2044.
[18] P. Ochsenbein, D. Mandon, J. Fischer, R. Weiss, R. Austin, K. Jayaraj, A. Gold, J. Terner, E. Bill, M. Muther, A.X. Trautwein, Angew. Chem., Int. Ed. Engl. 32 (1993) 1437.
[19] M.W. Grinstaff, M.G. Hill, E.R. Birnbaum, W.P. Schaefer, J.A. Labinger, H.B. Gray, Inorg. Chem. 34 (1995) 4896.
[20] W.P. Schaefer, J.A. Hodge, M.E. Hughes, H.B. Gray, J.E. Lyons, P.E. Ellis Jr., R.W. Wagner, Acta Crystallogr Sect. C (Cr. Str. Comm.) C49 (1993) 1342.
[21] E.R. Birnbaum, W.P. Schaefer, J.A. Labinger, J.E. Bercaw, H.B. Gray, Inorg. Chem. 34 (1995) 1751.
[22] E.R. Birnbaum, J.A. Hodge, M.W. Grinstaff, W.P. Schaefer, L. Henling, J.A. Labinger, J.E. Bercaw, H.B. Gray, Inorg. Chem. 34 (1995) 3625.
[23] G.A. Spyroulias, A. Despotopoulos, C.P. Raptopoulou, A. Terzis, A.G. Coutsolelos, J. Chem. Soc. Chem. Commun. (1997) 783.
[24] Zou Jian-Zhong, Li Ming, Xu Zheng, You Xiao-Zeng, Yu Kai-Bei, Jiegou Huaxue, J. Struct. Chem. 16 (1997) 29.
[25] K.M. Kadish, M. Autret, Zhongping Ou, P. Tagliatesta, T. Boschi, V. Fares, Inorg. Chem. 36 (1997) 204.
[26] Jian-Zhong Zou, Ming Li, Zheng Xu, Xiao-Zeng You, Hua-Qin Wang, Huaxue Xuebao, Acta Chim. Sinica, Chin. 52 (1994) 683.
[27] O.Q. Munro, H.M. Marques, P.G. Debrunner, K. Mohanrao, W.R. Scheidt, J. Am. Chem. Soc. 117 (1995) 935.
[28] M.A. Lopez, P.A. Kollman, J. Am. Chem. Soc. 111 (1989) 6212.
[29] S.R. Niketic, Kj. Rasmussen, The Consistent Force Field: A Documentation, Lecture Notes in Chemistry, vol. 3, Springer, Berlin, 1977.
[30] O.Q. Munro, J.C. Bradley, R.D. Hancock, H.M. Marques, F. Marsicano, P.W. Wade, J. Am. Chem. Soc. 114 (1992) 7218.
[31] A.K. Rappé, C.J. Casewit, Molecular Mechanics across Chemistry, University Science Books, Sausalito, California, 1997.
[32] S.R. Niketic, Kj. Rasmussen, Acta Chem. Scand. A32 (1978) 391.
[33] Kj. Rasmussen, Potential Energy Functions in Conformational Analysis, Lecture Notes in Chemistry, vol. 37, Springer, Berlin, 1985.
[34] N. Raos, S.R. Niketić, V. Simeon, J. Inorg. Biochem. 16 (1982) 1.
[35] J.H. Ammeter, H.B. Bürgi, J.C. Thibeault, R. Hoffmann, J. Am. Chem. Soc. 100 (1978) 3686.
[36] C. Mealli, D.M. Proserpio, J. Chem. Educ. 67 (1990) 399.
[37] J.H. Ammeter, H.B. Bürgi, J.C. Thibeault, R. Hoffmann, J. Am. Chem. Soc. 100 (1978) 3686 (Program CACAO [Computer Aided Composition of Atomic Orbitals], Version 3.0; based on the EHMO program SIMCON with weighted Wolfsberg–Helmholz formula).
[38] W. Jentzen, I. Turowska-Tyrk, W.R. Scheidt, J.A. Shelnutt, Inorg. Chem. 35 (1996) 3559.
[39] M.N. Burnett, C.K. Johnson, ORTEP-III: OAK RIDGE THERMAL ELLIPSOID PLOTTING PROGRAM FOR CRYSTAL STRUCTURE ILLUSTRATIONS, ORNL-6895, Oak Ridge Natl. Lab., Oak Ridge, Tennessee, July 1996.
[40] P. McArdle, J. Appl. Crystallogr. 27 (1994) 438.
[41] T. Van Zandt, PS-TRICKS: POSTSCRIPT MACROS FOR GENERIC TEX, Version 0.93a, User's Manual, Department of Economics, Princeton University, Princeton, NJ, 1993.
[42] M. Nardelli, J. Appl. Cryst. 28 (1995) 659 PARST: A System of Computer Routines for Calculating Molecular Parameters from the Results of Crystal Structure Analyses. (Version of 02/1997).
[43] M. Nardelli, A. Musatti, P. Domiano, G.D. Andreetti, Ric. Sci. 15 (II-A) (1965) 807.
[44] The following Cytochrome C3 coordinates were used: 1CZJ, 2CDV, 2CY3, 2CYM, and 1WAD.
[45] H.M. Berman, J. Westbrook, Z. Feng, G. Gilliland, T.N. Bhat, H. Weissing, I.N. Shindyalov, P.E. Bourne, The Protein Data Bank, Nucleic Acids Res 28 (2000) 235.
[46] J.A. Shelnutt, X. Song, J.G. Ma, S.L. Jin, W. Jentzen, C.J. Medforth, Chem. Soc. Rev. 27 (1998) 31.
[47] J.A. Shelnutt, http://jasheln.unm.edu/jasheln/content/nsd/nsd_oop_lookup.asp
[48] N.Y. Nelson, C.J. Medforth, D.J. Nurco, S.L. Jin, J.A. Shelnutt, K.M. Smith, J. Chem. Soc., Chem. Commun. (1999) 2071.